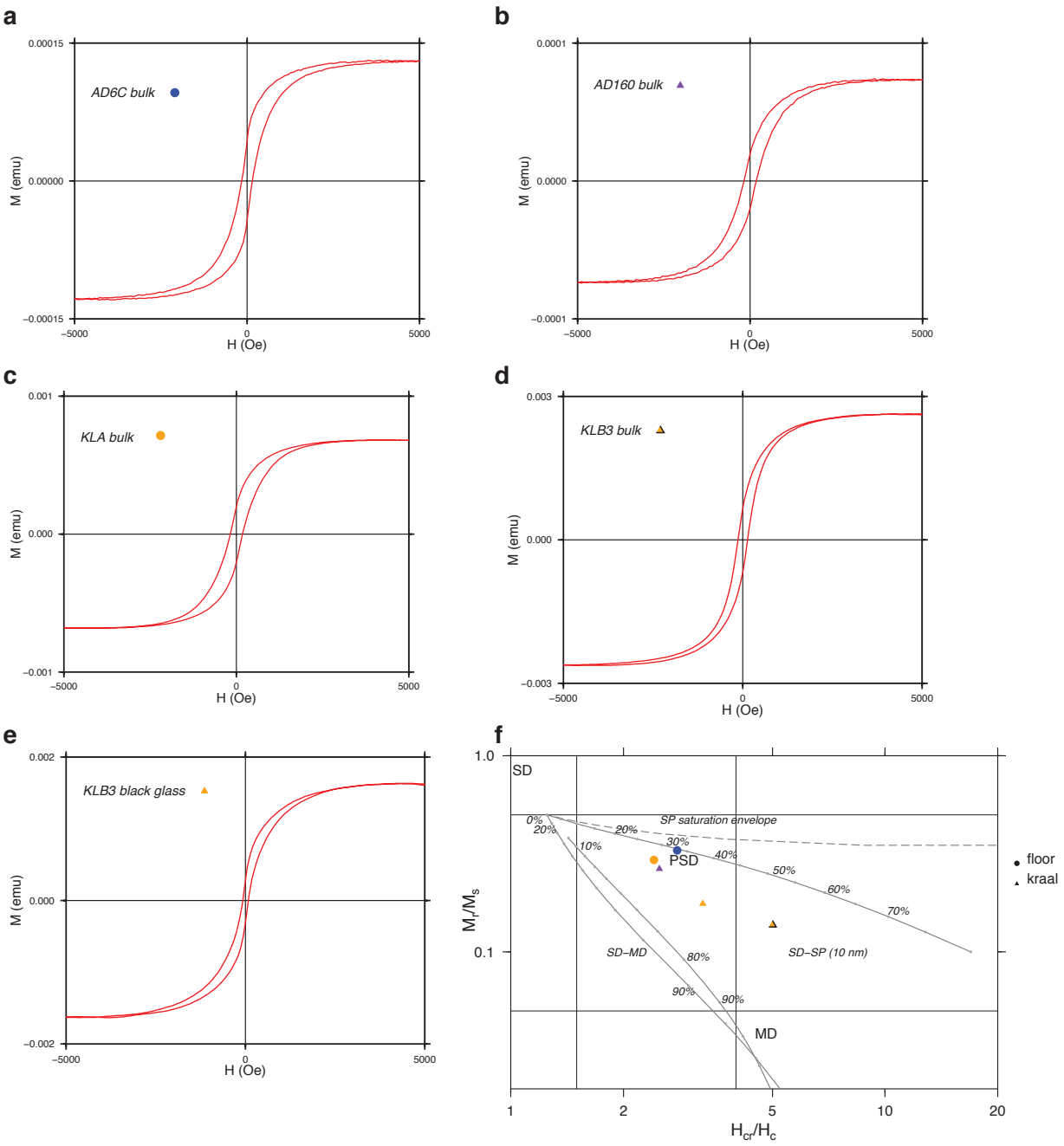

Supplementary Figure 1. Example magnetic hysteresis curves. **a**, Baobab burnt grain bin floor (AD6). **b**, Icon burnt kraal (AD160). **c**, Kolope burnt hut floor (KLA). **d**, Kolope burnt kraal (KLB). **e**, Kolope burnt kraal black glass. **f**, Data (**a-e**) shown on a Day plot. Abbreviations: SD, single domain; PSD, pseudo-single domain; MD, multidomain; M_r, saturation remanence; M_s, saturation magnetization; H_c, coercivity; H_{cr}, coercivity of remanence.

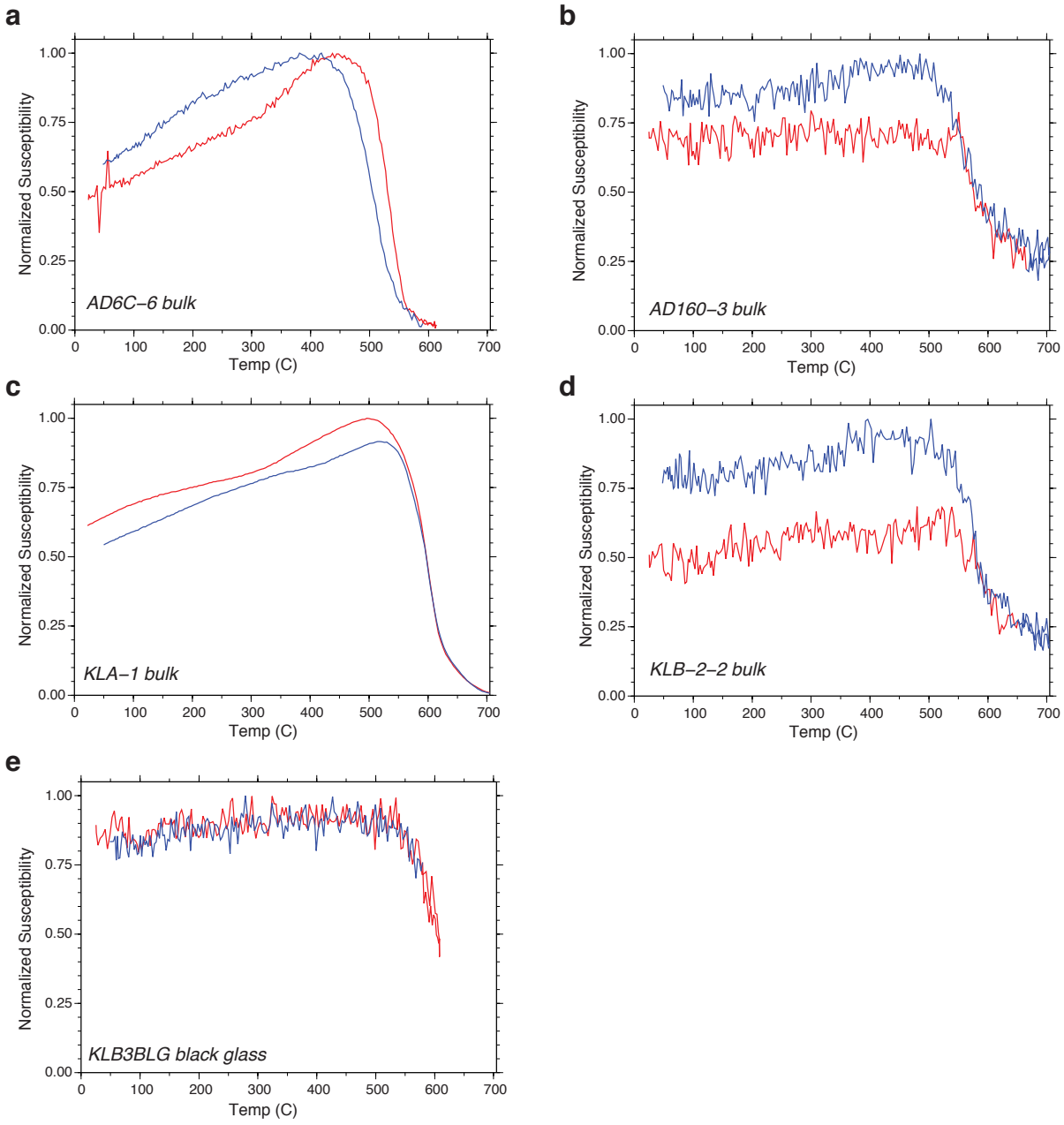

Supplementary Figure 2. Example magnetic susceptibility versus temperature data. Kraal samples generally have room temperature magnetic susceptibilities that are one to two orders of magnitude less than the hut and grain bin floor samples. **a**, Baobab burnt grain bin floor (AD6). **b**, Icon burnt kraal (AD160). **c**, Kolope burnt hut floor (KLA). **d**, Kolope burnt kraal (KLB). **e**, Kolope burnt kraal black glass. Red, heating curve, blue cooling curve.

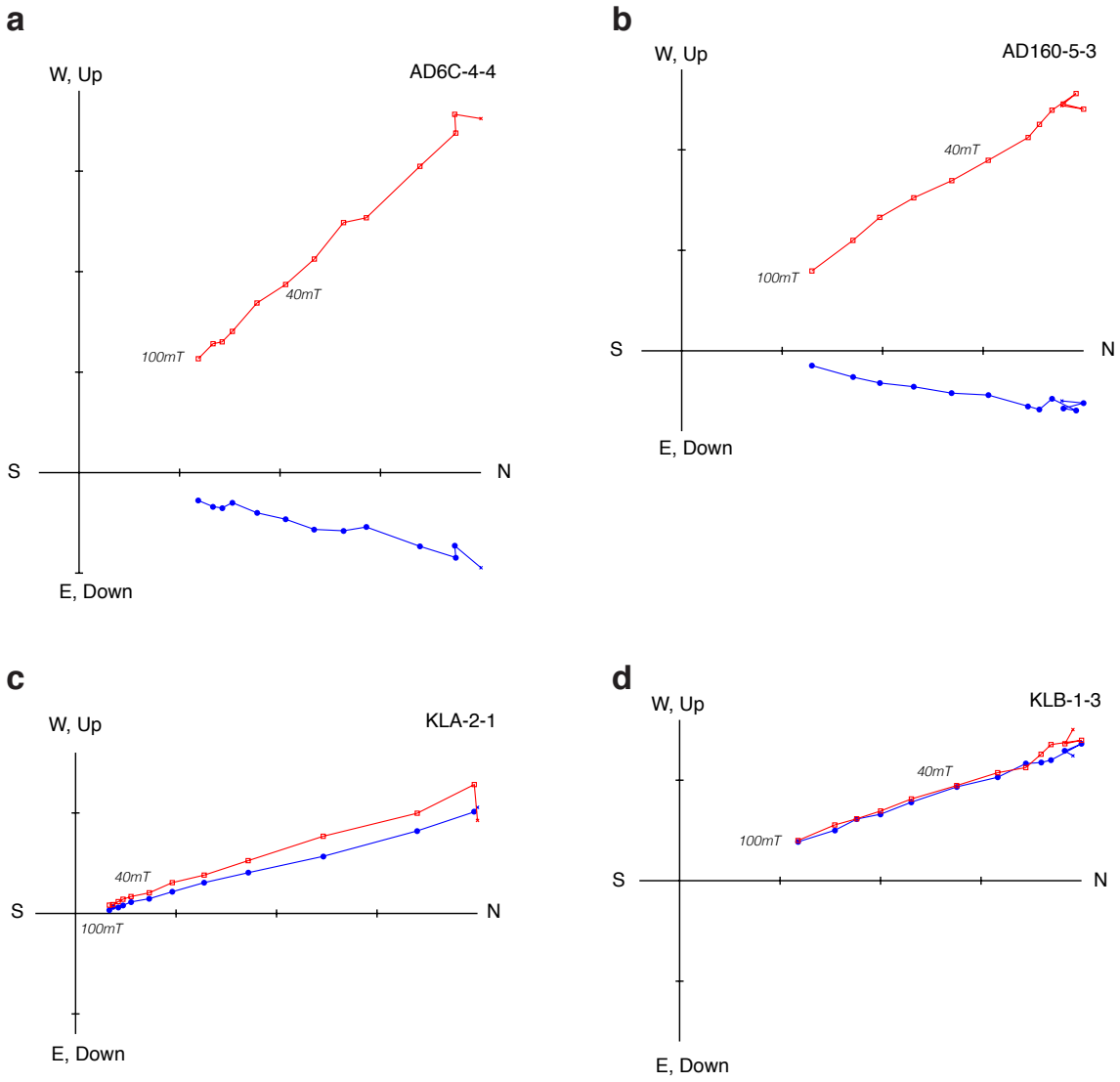

Supplementary Figure 3. Example orthogonal vector plots (stepwise alternating field demagnetization). Vertical projection is in red (inclination); horizontal projection is in blue (declination). **a**, Baobab burnt grain bin floor (AD6), NRM intensity = 8.78 x 10^{-7} A m^2. **b**, Icon burnt kraal (AD160), NRM intensity = 1.64 x 10^{-8} A m^2. **c**, Kolope burnt hut floor (KLA), NRM intensity = 6.40 x 10^{-7} A m^2. **d**, Kolope burnt kraal (KLB), NRM intensity = 1.70 x 10^{-8} A m^2.

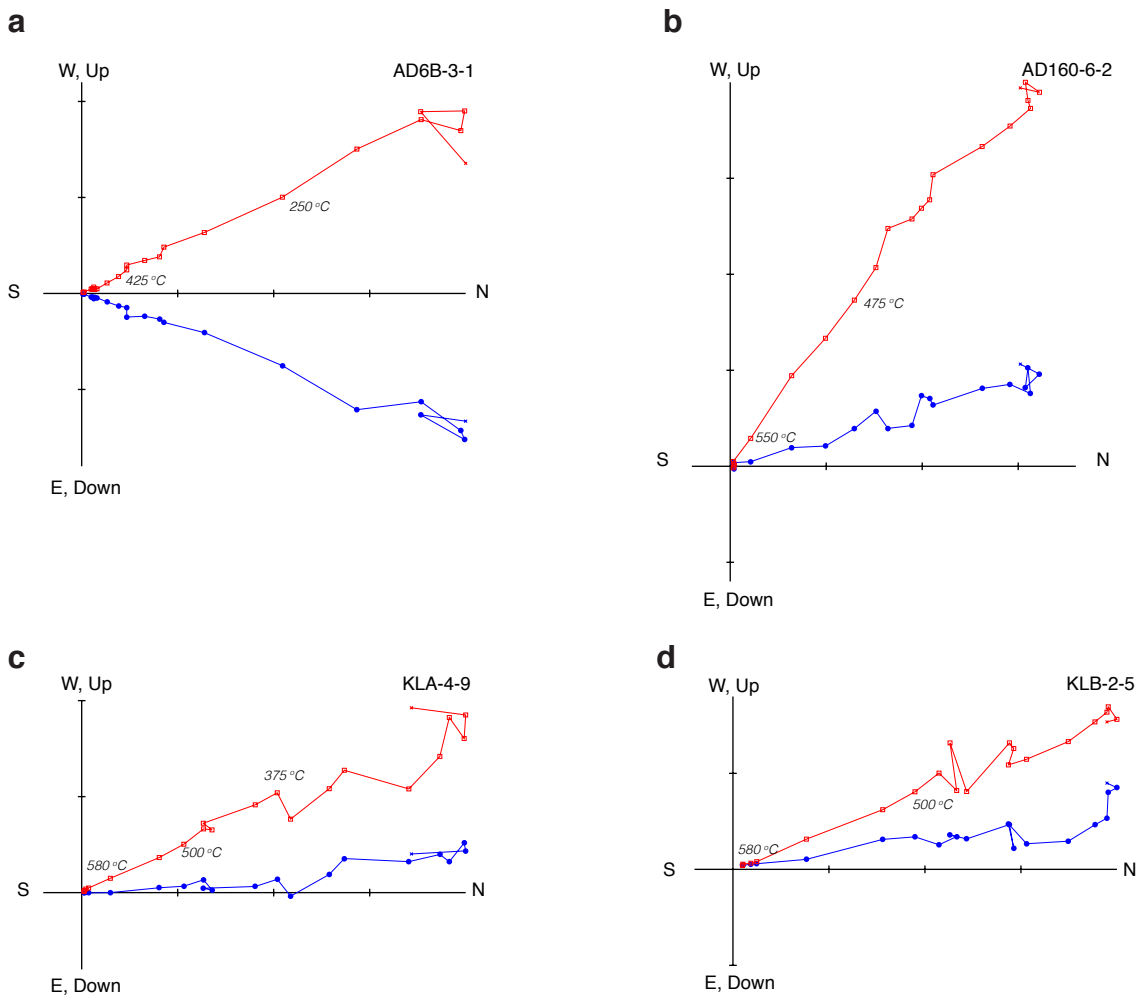

Supplementary Figure 4. Example orthogonal vector plots (stepwise thermal demagnetization). Vertical projection is in red (inclination); horizontal projection is in blue (declination). **a**, Baobab burnt grain bin floor (AD6), NRM intensity = 1.86 x 10^{-6} A m^2. **b**, Icon burnt kraal (AD160), NRM intensity = 4.51 x 10^{-8} A m^2. **c**, Kolope burnt hut floor (KLA), NRM intensity = 1.19 x 10^{-6} A m^2. **d**, Kolope burnt kraal (KLB), NRM intensity = 2.67 x 10^{-8} A m^2.

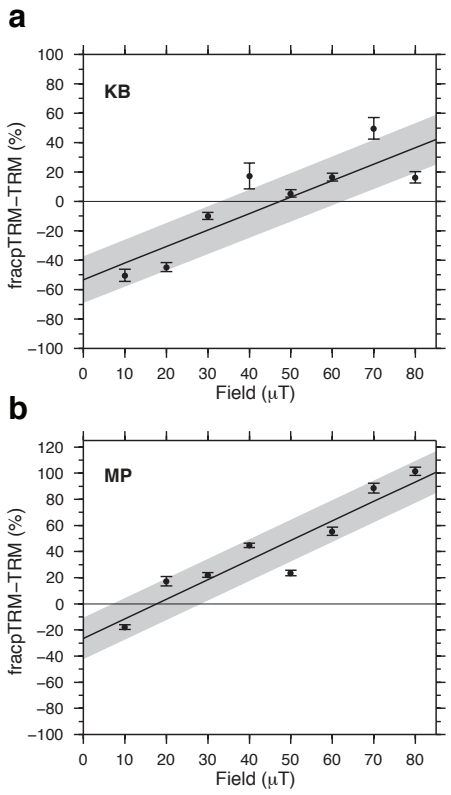

Supplementary Figure 5. Example multi-specimen paleointensity results from ceramics. Uncertainties on individual analyses combine, using propagation of errors, uncertainties in NRM and measurement after heating to 300 ^{o}C (1 σ). Uncertainties on line fit are from jackknife-1 analyses (1σ). **a**, Klingbiel (KB). **b**, Mapungubwe (MP).

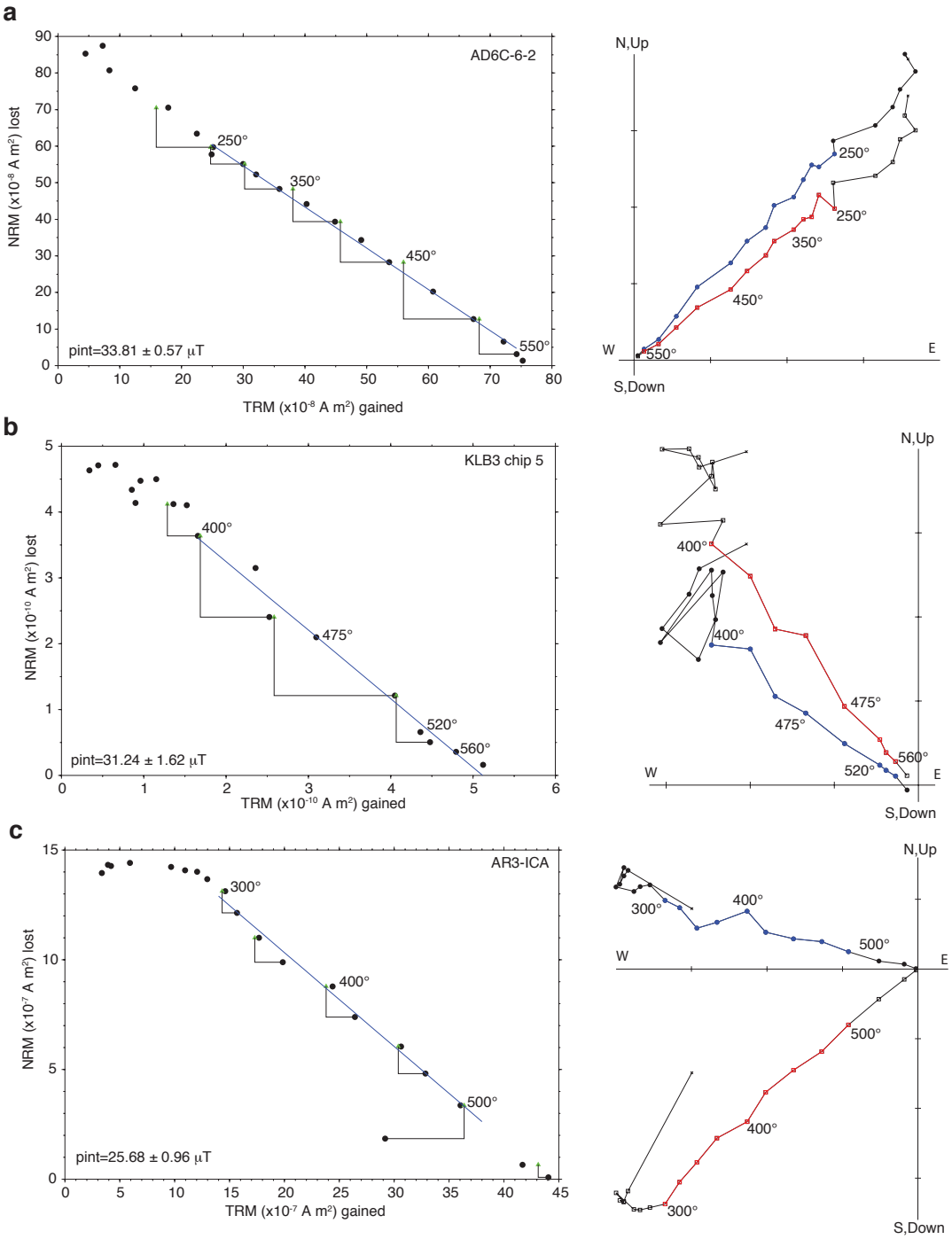

Supplementary Figure 6. Thellier-Coe paleointensity plots for representative samples from baked floors and kraals. **a**, Baobab burnt grain bin floor (AD6). Left, natural remanent magnetization (NRM) vs. thermoremanent magnetization (TRM). Right, Orthogonal vector plot of field-off steps (coloured segments highlight temperature range used for paleointensity determination). **b**, Kolope burnt kraal black glass, conventions as in (**a**). **c**, Icon ceramic, conventions as in (**a**).

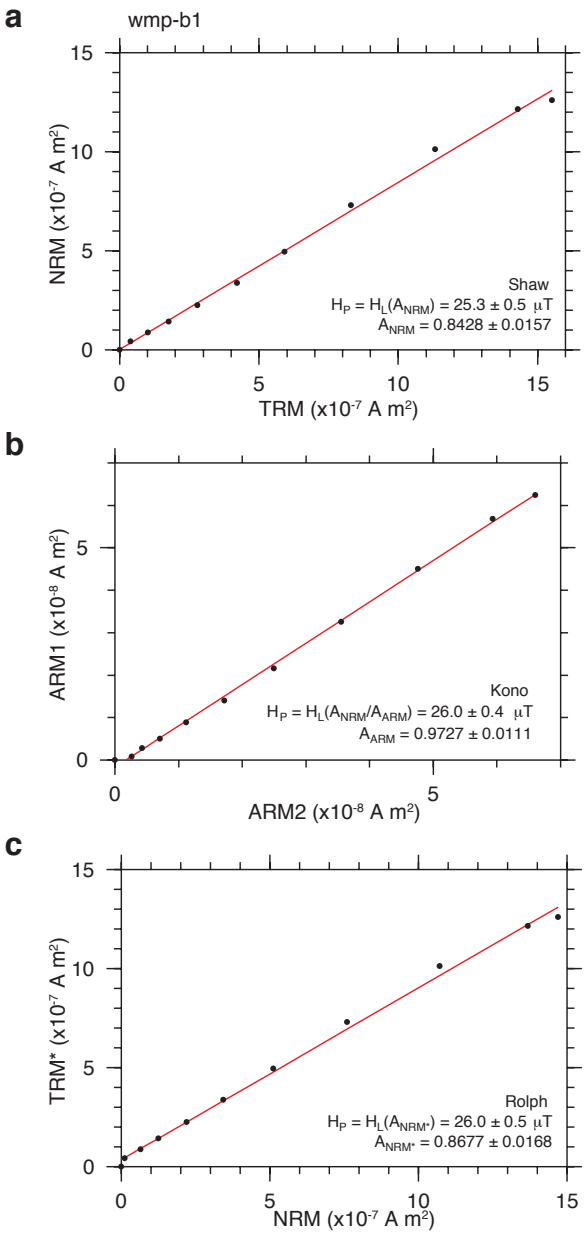

Supplementary Figure 7. Example Shaw paleointensity plots. Analyses of Icon ceramic shown using **a**, Shaw method, with **b**, Kono and **c**, Rolph correction applied. Abbreviations: NRM, natural remanent magnetization; ARM, anhysteretic magnetization.

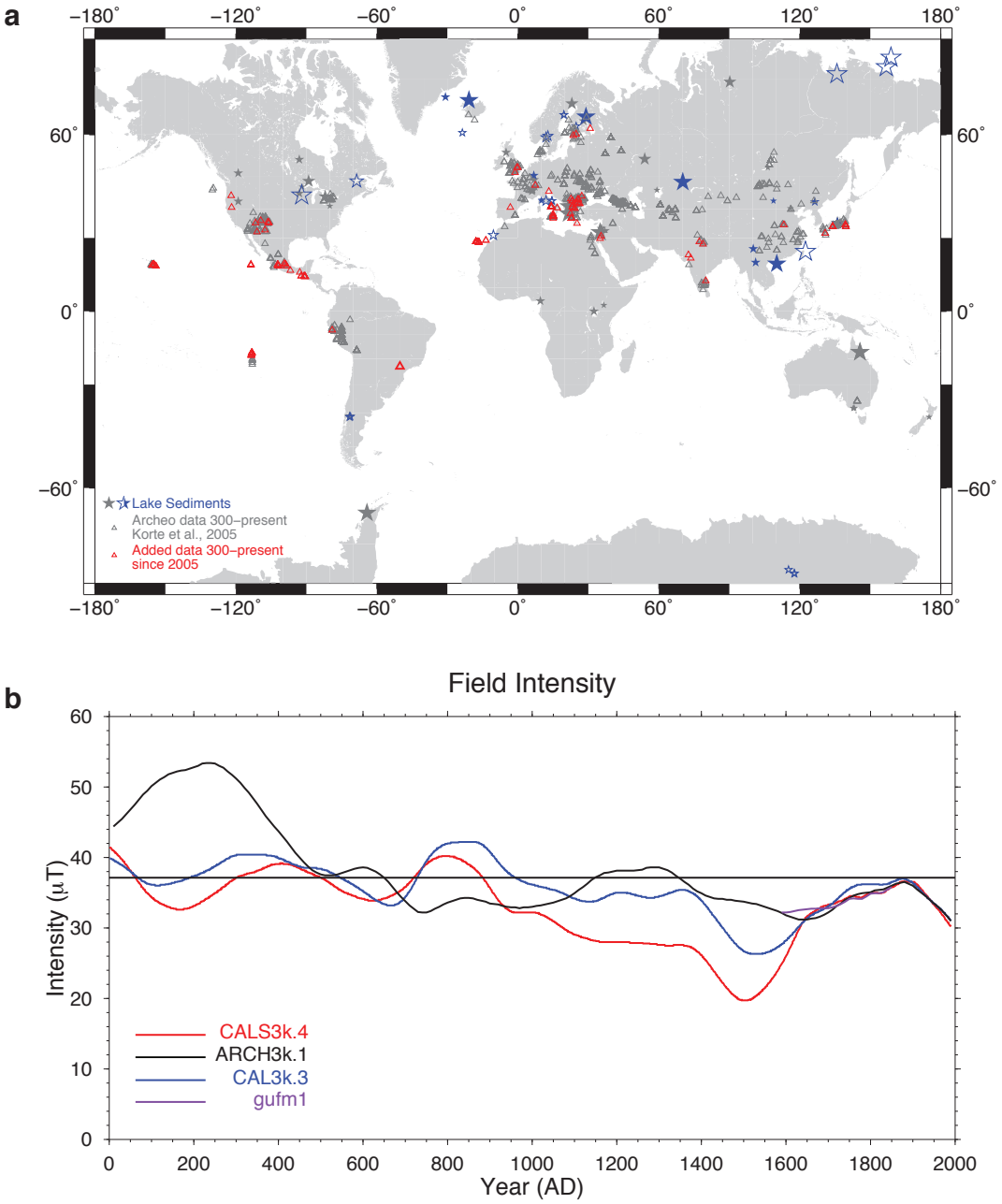

Supplementary Figure 8. Archeological, lava and sediment data used in models together with model predictions for southern Africa. **a**, Data spanning 300 AD to present. Gray symbols are sediment directions (stars) and archeological data (triangles) used in models by Korte et al.[18]. Blue stars represent sediment directions (closed) and sediment calibrated intensities (open) added by Donadini et al.[17] and Korte and Constable[16]. Red triangles represent archeological data, data from lavas and data from submarine basaltic glass added by Donadini et al.[17] and Korte and Constable[16]. **b**, Paleointensity for southern Africa predicted by various models (gufm[20], CAL3k.3[17], ARCH3k.1[17], CALS3k.4[16]).

Supplementary Table 1: Summary Paleomagnetic directional data.
Dec, declination; Inc, inclination; N, number of samples analyzed, n, number of floor pieces collected at site; n in site mean entry is the number sites. Icon result is based on analysis of one vitrified kraal.

Locality	Site	Type	Age (AD)	N *(n)*	Dec (^{o})	Inc (^{o})	k	α^o_{95}
Baobab	AD6A	grain bin	1013-1047	15	19.9	-27.6	50	5.5
				6	20.2	-26.9	54	9.2
Baobab	AD6B	grain bin	1013-1047	14	22.6	-32.7	78	4.5
				6	22.1	-33.3	75	7.8
Baobab	AD6C	grain bin	1013-1047	18	19.9	-32.6	20	7.8
				6	21.1	-30.2	14	18.5
Baobab mean			1013-1047	*3*	21.1	-30.1	602	5.0
Icon (Venetia)	AD160	kraal	1317-1415	14	0.6	-42.9	37	6.6
Kolope	KLA	hut	1507-1585	10	351.2	-23.0	80	5.4
				4	350.4	-21.9	82	10.2
Kolope	KLB	kraal	1507-1585	8	347.6	-22.1	152	4.5
Kolope mean			1507-1585	*2*	349.0	22.0	1937	5.7

Supplementary Table 2: Paleomagnetic directional data, Kolope KLA AF, alternating field demagnetization, Th, thermal demagnetization; Steps, demagnetization steps used in principal component analysis (PCA), +0, origin used in PCA fit; N, number of steps used in PCA fit; MAD, maximum angular deviation of PCA fit.

Sample	Method	Steps	N	Dec (^{o})	Inc (^{o})	MAD (^{o})
KLA-1-4	AF	p25.0-100.0+0	9	347.4	-21.3	2.2
KLA-1-5	AF	p25.0-100.0+0	9	347.8	-15.0	2.0
KLA-2-1	AF	p20.0-100.0+0	10	345.7	-16.8	1.9
KLA-2-4	AF	p30.0-100.0+0	8	345.0	-13.7	1.6
KLA-3-2	Th	p525.0-650.0+0	7	3.2	-33.6	3.2
KLA-3-3	AF	p20.0-100.0+0	10	354.3	-31.1	2.1
KLA-3-4	AF	p25.0-100.0+0	9	358.6	-30.6	1.8
KLA-4-9	Th	p500.0-650.0+0	8	356.3	-24.6	1.3
KLA-4-10	AF	p50.0-100.0+0	6	346.6	-23.9	2.5
KLA-4-13	AF	p40.0-100.0+0	7	349.9	-17.9	1.3

Supplementary Table 3: Paleomagnetic directional data, Kolope KLB
Abbreviations as in Supplementary Table 2.

Sample	Method	Steps	N	Dec (^{o})	Inc (^{o})	MAD (^{o})
KLB-1-1	AF	p50.0-100.0+0	6	343.1	-17.5	3.7
KLB-1-2	Th	p500.0-650.0+0	8	350.0	-16.5	8.3
KLB-1-3	AF	p40.0-100.0+0	7	341.2	-18.2	1.0
KLB-2-1	AF	p40.0-100.0+0	7	344.8	-24.1	1.2
KLB-2-3	AF	p50.0-100.0+0	6	350.2	-18.5	2.5
KLB-2-5	Th	p500.0-650.0+0	8	350.1	-22.4	1.9
KLB-3-3	AF	p20.0-50.0+0	6	350.7	-28.3	7.6
KLB-3-7	AF	p30.0-70.0+0	6	351.6	-31.2	7.9

Supplementary Table 4: Paleomagnetic directional data, Icon AD160
Abbreviations as in Supplementary Table 2.

Sample	Method	Steps	N	Dec (^{o})	Inc (^{o})	MAD (^{o})
AD160-1-1	AF	p40.0-100.0+0	7	5.6	-61.5	2.9
AD160-1-4	AF	p40.0-100.0+0	7	5.8	-58.6	1.9
AD160-2-1	AF	p50.0-100.0+0	6	1.3	-27.7	1.8
AD160-2-2	Th	p500.0-580.0+0	6	1.0	-32.9	2.4
AD160-2-3	AF	p60.0-100.0+0	5	3.9	-32.9	2.4
AD160-3-1	AF	p50.0-100.0+0	6	2.7	-41.5	3.4
AD160-3-2	AF	p50.0-100.0+0	6	359.5	-37.7	1.3
AD160-4-1	AF	p15.0-100.0+0	11	6.5	-46.1	4.4
AD160-4-8	AF	p40.0-100.0+0	7	13.5	-41.8	2.0
AD160-5-3	AF	p40.0-100.0+0	7	8.8	-32.1	2.0
AD160-5-4	AF	p40.0-100.0+0	7	7.2	-29.0	1.9
AD160-6-1	AF	p60.0-100.0+0	5	335.9	-48.9	1.1
AD160-6-2	Th	p475.0-580.0+0	7	345.0	-52.6	2.4
AD160-6-5	AF	p50.0-100.0+0	6	343.6	-51.7	1.4

Supplementary Table 5: Paleomagnetic directional data, Baobab AD6
Abbreviations as in Supplementary Table 2.

Sample	Method	Steps	N	Dec (^{o})	Inc (^{o})	MAD (^{o})
AD6A-1-1	AF	p20.0-70.0+0	7	34.3	-41.8	1.2
AD6A-1-5	AF	p40.0-100.0	6	24.0	-40.1	5.4
AD6A-1-6	AF	p40.0-100.0+0	7	27.1	-38.6	4.1
AD6A-2-1	AF	p40.0-100.0+0	8	18.2	-15.6	1.2
AD6A-2-5	AF	p20.0-40.0+0	5	15.2	-22.9	3.6
AD6A-2-6	AF	p60.0-100.0+0	5	6.5	-24.3	2.1
AD6A-3-5	Th	p475.0-580.0+0	7	21.0	-29.0	1.7
AD6A-3-6	AF	p30.0-100.0+0	8	11.2	-38.3	3.9
AD6A-3-8	AF	p30.0-100.0+0	8	15.5	-23.4	4.6
AD6A-4-2	AF	p20.0-100.0+0	10	12.6	-12.7	2.4
AD6A-4-4	AF	p40.0-80.0+0	6	16.9	-13.2	2.8
AD6A-5-4	AF	p40.0-100.0+0	7	28.1	-28.5	5.4
AD6A-5-5	AF	p30.0-100.0+0	8	29.3	-23.1	2.0
AD6A-6-3	AF	p40.0-100.0+0	7	23.6	-29.4	1.1
AD6A-6-4	AF	p40.0-100.0+0	7	19.5	-30.7	2.9
AD6B-1-3	AF	p10.0-100.0	12	17.1	-37.8	1.1
AD6B-1-5	AF	p20.0-60.0+0	7	22.0	-37.9	3.6
AD6B-3-1	Th	p425.0-580.0+0	9	17.4	-26.0	4.5
AD6B-3-3	AF	p30.0-60.0+0	5	25.5	-24.4	2.1
AD6B-3-4	AF	p20.0-50.0+0	6	20.4	-25.2	2.4
AD6B-4-7	AF	p25.0-100.0+0	9	27.1	-44.1	3.0
AD6B-4-8	AF	p40.0-100.0+0	7	33.2	-36.3	2.6
AD6B-5-1	AF	p30.0-100.0+0	8	14.2	-22.7	3.6
AD6B-5-3	AF	p30.0-100.0+0	8	10.4	-22.9	2.5
AD6B-6-1	AF	p30.0-100.0+0	8	30.3	-37.6	3.8
AD6B-6-2	AF	p20.1-100.0+0	11	29.5	-29.9	1.1
AD6B-6-4	AF	p40.0-100.0+0	8	27.1	-31.7	2.3
AD6B-7-1	AF	p30.0-100.0+0	8	23.5	-41.3	2.0
AD6B-7-2	AF	p20.0-80.0+0	9	21.2	-37.7	3.6

(Supplementary Table 5 continued)

Sample	Method	Steps	N	Dec (^{o})	Inc (^{o})	MAD (^{o})
AD6C-1-2	AF	p20.1-100.0+0	11	14.6	-32.3	1.7
AD6C-1-4	AF	p30.0-100.0+0	10	14.3	-36.9	2.7
AD6C-1-5	AF	p20.0-60.0+0	7	8.2	-38.2	3.9
AD6C-2-1	AF	p30.0-100.0+0	9	13.4	-37.5	1.4
AD6C-2-6	AF	p25.0-100.0+0	11	17.7	-30.9	2.1
AD6C-2-8	AF	p25.0-100.0+0	9	8.0	-41.6	4.8
AD6C-3-3	AF	p50.0-100.0+0	7	15.2	-30.3	2.0
AD6C-3-4	AF	p30.0-80.0+0	7	12.4	-35.1	5.8
AD6C-3-5	AF	p50.0-80.0+0	5	15.7	-33.6	1.7
AD6C-3-9	AF	p20.0-70.0+0	8	14.9	-38.9	2.9
AD6C-4-1	AF	p20.1-80.0+0	9	16.5	-45.7	2.7
AD6C-4-3	AF	p20.0-70.0+0	8	14.0	-45.0	2.7
AD6C-4-4	AF	p30.0-80.0+0	7	13.1	-41.6	2.2
AD6C-5-1	AF	p25.0-100.0+0	10	36.1	16.3	2.1
AD6C-5-7	AF	p20.0-100.0+0	10	29.2	5.1	2.8
AD6C-6-1	AF	p50.0-100.0+0	7	37.6	-38.0	2.3
AD6C-6-5	AF	p40.0-70.0+0	5	36.6	-33.1	1.1
AD6C-6-6	AF	p40.0-100.0+0	7	33.6	-34.4	3.5

Supplementary Table 6: Multi-specimen method paleointensity data on ceramics
†See Figure 2 of main text.

Abbreviation†	Locality	Age (AD)	Paleointensity (μT)
KB	Klingbiel	1000-1200	$47.48\ ^{-9.36}_{+11.7}$
MP	Mapungubwe	1250-1325	$17.68\ ^{-3.52}_{+3.98}$
GZ	Great Zimbabwe/Chibvumani	1450-1700	$37.06\ ^{-5.38}_{+6.21}$
IC	Icon	1317-1415	$9.02\ ^{-1.92}_{+2.15}$
LT	Letaba	1600-1840	$34.79\ ^{-16.45}_{+31.45}$
RB	Rooiberg	1650-1750	$39.20\ ^{-11.65}_{+18.4}$
BP	Buispoort	1700-1840	$48.87\ ^{-23.08}_{+46.16}$

Supplementary Table 7: Summary paleointensity data (Thellier-Coe and Shaw methods) †See Figure 2 of main text. *Thellier-Coe mean value from Neukirch et al.[21]. N, number of samples used in mean. ‡See Table Supplementary Table 8 for sample results.

Abbreviation†	Localities	Material	Age (AD)	N	Paleointensity (μT)‡
AD6	Baobab	grain bins	1013-1047	3	34.97 ±1.59
AD300/198*	AD300/198	grain bins	1200-1250	11	32.6 ±3.6
MP	Mapungubwe,Weipe	ceramics	1250-1325	3	22.15 ±3.51
IC	Icon,Matoks	ceramics	1317-1442	4	22.88 ±2.00
KLB	Kolope	kraal glass	1507-1585	4	29.90 ±1.15

Supplementary Table 8: Thellier-Coe and Shaw method sample paleointensity results

†Abbreviation used in Figure 2 of main text and Supplementary Table 7. N, number of points used in paleointensity determination; T, temperature range used in paleointensity determination; T-C, Thellier-Coe paleointensity method; S-R, Shaw-Rolph pqaleointensity method; Atm., atmosphere used during the experiment; b, slope of linear fit in paleointensity plots of NRM lost versus laboratory TRM gained; σ_b, error in the linear fit; f, g, q, Coe et al.[11] quality factors for Thellier-Coe determinations.

Locality	Sample	Material	N	T (^{o}C)	Paleointensity (μT)	Method	Atm.	b	σ_b	f	g	q
AD6†												
Baobab	ad6c-2-3	grain bin	13	250-550	36.75 ± 1.05	T-C	Air	-1.223	0.032	0.394	0.847	12.8
Baobab	ad6c-4-2	grain bin	10	325-550	34.15 ± 1.11	T-C	Air	-1.135	0.040	0.541	0.878	13.5
Baobab	ad6c-6-2	grain bin	13	250-550	33.91 ± 0.57	T-C	Air	-1.127	0.019	0.444	0.867	22.8
MP†												
Mapungubwe	ar2-mpb	ceramic	5	450-550	19.14 ± 0.78	T-C	Ar	-0.311	0.010	0.556	0.730	12.6
Mapungubwe/Weipe	wmp-a3	ceramic	10		21.34 ± 1.07	S-R	Air					
Mapungubwe/Weipe	wmp-b1	ceramic	11		26.03 ± 0.78	S-R	Air					
IC†												
Icon/Matoks	ic-b1	ceramic	4	500-580	22.96 ± 1.84	T-C	Ar	-0.574	0.046	0.301	0.652	2.45
Icon/Venetia	ar3-ica	ceramic	9	300-500	25.68 ± 0.96	T-C	Air	-0.428	0.016	0.624	0.866	14.5
Icon/Matoks	ic-a2	ceramic	4	450-525	21.30 ± 2.32	T-C	Air	-0.533	0.058	0.386	0.571	2.03
Icon/Matoks	ic-a3	ceramic	9		21.60 ± 1.30	S-R	Air					
KLB†												
Kolope	klb3-ch2	kraal glass	8	400-560	28.69 ± 2.12	T-C	Air	-0.956	0.071	0.154	0.774	1.61
Kolope	klb3-ch3	kraal glass	5	450-540	32.34 ± 1.27	T-C	Air	-1.078	0.042	0.330	0.619	5.23
Kolope	klb3-ch4	kraal glass	8	400-560	27.34 ± 1.13	T-C	Air	-0.911	0.038	0.395	0.777	7.37
Kolope	klb3-ch5	kraal glass	9	400-580	31.24 ± 1.62	T-C	Air	-1.041	0.054	0.677	0.802	10.5

Supplementary Note 1

Burnt Structures. The Iron Age brackets the last 2000 years in southern Africa. During this time, Bantu-speaking agriculturalists dominated the landscape. Their domestic economy included herding cattle, sheep and goats; cultivating various sorghums, millets, beans and peas; and residence in semi-permanent villages that included animal kraals (byres) together with pole-and-daga (mud) houses and grain bins. Sometimes these daga structures were burnt down as a ritual of cleansing during sustained droughts[1,2]. As a rule, if grain bins were intentionally burnt, cultivation was in crisis. Similarly, if kraals were burnt, domestic animals were dying unexpectedly. In this case, animal enclosures were probably burnt for both hygienic and ritual purposes. We sampled three new sites with these burnt features.

The Baobab (2229AD6) Middle Iron Age site (Longitude 29.29^o E, Latitude 22.31^o S) sits on top of the Edmondsburg ridge in the Venetia Game Reserve[3]. The pottery belongs to the Zhizo facies that dates to between AD 750 and 1050[1]. The Baobab homestead dates to the end of this period at AD 910±40 (Pta 7450). (Note, "Pta" refers to the Pretoria geochronology lab sample number.) This date calibrates to AD 996-1134 using SHCal13[4]. Based on the stratigraphic sequence within the valley, the most likely span is AD 1013-1047. Heavy rains have exposed multiple arcs of at least 40 burnt grain bins; we sampled three.

The Icon (Venetia, 2229AD160) Late Iron Age site (Longitude 29.28^o E, Latitude 22.31^o S) is one of five homesteads with central cattle kraals at the base of the Edmondsburg ridge below the Baobab site. The pottery belongs to the Icon facies, dating from AD 1300 to 1500[1]. This homestead is not yet dated but the nearby name site dates to cal AD 1317-1415[5] (Pta 1652) using SHCal13. On the basis of the age of the nearby homestead and the occurrence of Icon facies ceramics, we adopt an age of AD 1317-1415 for the Icon (Venetia) site. We sampled the rim of the main vitrified cattle kraal.

The Kolope (2229AD4) Late Iron Age site (Longitude 29.27^o E, Latitude 22.31^o S) is located in the saddle of the Edmondsburg ridge. The pottery belongs to the Khami facies, dating to between AD 1400 and 1820[1]. This homestead has been dated to 340 ±40 BP (Pta 7975), which calibrates at one sigma to AD 1507-1640. Based on the stratigraphic sequence within the valley, the most likely span is AD 1507-1585. We sampled a burnt hut floor and the rim of a vitrified cattle kraal.

Ceramics. Successful high-resolution (Thellier-Coe) results were obtained only for Icon and Mapungubwe facies ceramics; sample localities are described below.

The Matoks (2329BC2) Late Iron Age site was exposed by road operations at the Tropic of Capricorn about 140 km south of Mapungubwe. The pottery belongs to the Icon facies and has been radiocarbon dated to 570 ±50 BP (Pta 7330) which calibrates to AD 1392-1442 using SHCal13.

The Weipe 508 (2229AB508) Middle Iron Age site is located next to the Limpopo floodplain only a few km east of Mapungubwe. A Transitional level lies underneath a Mapungubwe homestead that has been dated to 630 ±70 BP (Pta 9549) which calibrates to AD 1307-1414 using SHCal13. It thus dates to the end of the Mapungubwe period, that is to between AD 1300 and 1325.

Mapungubwe (2229AB1) was the capital of the first pre-colonial state in southern Africa. Famous for golden objects discovered in the 1930s[6], it was a rainmaking hill before the capital shifted there from the site K2 one kilometer away. Consequently, several Early and Middle Iron Age pottery facies are stratified in the deposits[1]. Three radiocarbon dates (Pta 752, Pta 1209 and Pta 6692) bracket Mapungubwe pottery to between AD 1250 and 1325, or slightly longer[1].

Ceramics used for low-resolution paleointensity study (but failing to yield high resolution values after application of selection criteria) include Buispoort (1700-1840 AD), Letaba (1600-1840 AD), Rooiberg (1650-1750 AD), Great Zimbabwe/Chibvumani (1450-1700) and Klingbiel (1000-1200 AD). See Huffman[1] for further descriptions and age constraints.

Supplementary Methods

Field collection and paleointensity sample characteristics. Burnt floor samples were collected in the field and oriented with Sun and Brunton compasses. Large, systematic discrepancies indicative of local magnetic sources were not seen at the collection sites; the Brunton compass orientations were subsequently used for further analyses.

Standard 1-cc samples (identical to those used for directional analyses) were selected from the Baobab (AD6) site for paleointensity analyses. Bulk samples from the Kolope burnt grain bin had heterogeneity (i.e. small pebble size clasts) and thus were not used for paleointensity investigation. Paleointensity analyses of the Kolope kraal were restricted to black glass separated from larger bulk samples. Black glass was too small in our samples of the Icon (Venetia) byre for paleointensity analyses.

Paleointensity analyses. For successful paleointensity experiments on ceramics and burnt floors, the applied field was at a high angle ($\sim$50-125^o) to the natural remanent magnetization (NRM); linearity of the NRM/TRM slope under these conditions provides further support for minimal

influence of multidomain grains.

Modern pottery using traditional methods is made in the Venda region of southern Africa today. Pottery is fired in shallow pits. The temperatures measured in pit fires often reach 800 ^{o}C[7], but there is a range (typically 700-900 ^{o}C) due to variables in the local firing.

From our inquires with modern potters, we found that the heating and cooling process generally takes ∼12 hours. We note that this total time is within a factor of 2 of the total heating/cooling time of a Thellier experiment on pottery shards and therefore we have not applied cooling rate corrections. Our cooling rates for paleointensity experiments are much faster than those for bulk samples, however we note that the glass must have cooled at much faster rates. We also note that several investigations indicate that cooling rate corrections for pseudo-single domain grains, similar to those that likely dominated our samples (cf. Supplementary Figure 1), are negligible[8−9].

Paleointensity success rates. Our selection criteria are similar to or more stringent than those summarized by Paterson et al.[10]. The low success rate of Thellier-Coe paleointensity results for pottery samples can be traced to multiple criteria that were failed. Failure of pTRM checks was the primary reason for failure (∼60%). A lack of linearity in the NRM-TRM plots also account for a large percentage of failed samples (∼50%). Several samples (∼30%) showed multiple magnetic components during demagnetization. Approximately 20% of samples showed principal components that did not trend towards the origin and ∼20% did not demonstrate a stable demagnetization during heating. Of the 11 samples that were examined using variations of the Shaw techniques, only 3 (27%) showed linear behavior with no low coercivity outliers. The burnt floor samples were better suited for paleointensity determinations. Hut and grain bin floor samples containing large pebbles were excluded from paleointensity analyses. Of the burnt floor samples analyzed, 60% passed all selection criteria, whereas 80% of kraal black glass passed all selection criteria. Coe et al.[11] statistics for accepted samples are summarized in Supplementary Table 7.

Anisotropy. We carried out a set of experiments to examine potential effects of thermoremanent magnetization (TRM) anisotropy[12−13]. One cube from pot shards AR2-MPB, AR3-ICA, IC-A and IC-B and 2 cubes from floor AD6C-6 were analyzed. A large portion of the specimens' natural remanent magnetization (NRM) was first removed by zero-field heating to 500°C. This temperature was chosen based on the demagnetization behavior observed during Thellier-Coe experiments. A series of six orthogonal TRM's were then imparted by heating to 500 ^{o}C in a 30 μT field ($+X$, $+Y$, $+Z$, $-X$, $-Y$, and $-Z$). In the sample coordinate system, $+X$ points orthogonally away from the pot shard surface, with the $Y-Z$ plane defined by the surface of the pot shard. For floor samples,

$+Z$ is orthogonal to the surface of the floor, with the $X-Y$ plane defined by the surface of the floor. Sample magnetization moment was monitored for significant changes in intensity that might indicate alteration of the sample. The sample from AR2-MPB showed the most variability, but no sample showed a systematic increase of magnetization with successive heatings.

Anisotropy tensors ($\boldsymbol{\kappa}$) were used to generate unit vectors in the corrected paleofield direction ($\hat{\mathbf{h}}$) and intensity correction factors[14] (f_{An}) for samples yielding successful Thellier-Coe paleointensity data. The anisotropy tensor in terms of the components of TRM, M_i (A m^2), resulting from heating in a laboratory field with components, H_{Li} (A/m), is given by,

$$M_i = \boldsymbol{\kappa}_{ij} H_{Li}. \tag{1}$$

Tensors are as follows:

$$\boldsymbol{\kappa}_{\mathrm{ADC6-6a}} = C_{\mathrm{ad6c-6a}} \begin{bmatrix} 1.000 & -0.035 & -0.008 \\ -0.035 & 0.958 & -0.023 \\ -0.008 & -0.023 & 0.925 \end{bmatrix},$$

$$\boldsymbol{\kappa}_{\mathrm{AD6C-6b}} = C_{\mathrm{ad6c-6b}} \begin{bmatrix} 1.000 & 0.087 & 0.005 \\ 0.087 & 0.936 & -0.062 \\ 0.005 & -0.062 & 0.953 \end{bmatrix},$$

$$\boldsymbol{\kappa}_{\mathrm{AR2-MPB}} = C_{\mathrm{ar2-mpb}} \begin{bmatrix} 1.000 & 0.037 & 0.014 \\ 0.037 & 1.167 & 0.128 \\ 0.014 & 0.128 & 0.934 \end{bmatrix},$$

$$\boldsymbol{\kappa}_{\mathrm{AR3-ICA}} = C_{\mathrm{ar3-ica}} \begin{bmatrix} 1.000 & -0.093 & 0.052 \\ -0.093 & 1.419 & -0.134 \\ 0.052 & -0.134 & 1.275 \end{bmatrix},$$

$$\boldsymbol{\kappa}_{\mathrm{IC-A2}} = C_{\mathrm{ic-a2}} \begin{bmatrix} 1.000 & 0.049 & -0.036 \\ 0.049 & 1.281 & 0.078 \\ -0.036 & 0.078 & 1.213 \end{bmatrix},$$

$$\boldsymbol{\kappa}_{\mathrm{IC-B1}} = C_{\mathrm{ic-b1}} \begin{bmatrix} 1.000 & -0.026 & -0.019 \\ -0.026 & 1.188 & 0.110 \\ -0.019 & 0.110 & 1.163 \end{bmatrix},$$

where $C_{\mathrm{ad6c-6a}} = 1.765 \times 10^{-8}$ m^3, $C_{\mathrm{ad6c-6b}} = 1.222 \times 10^{-8}$ m^3, $C_{\mathrm{ar2-mpb}} = 0.744 \times 10^{-8}$ m^3, $C_{\mathrm{ar3-ica}} = 3.558 \times 10^{-8}$ m^3, $C_{\mathrm{ic-a2}} = 0.352 \times 10^{-8}$ m^3, and $C_{\mathrm{ic-b1}} = 0.418 \times 10^{-8}$ m^3 are constants factored out for clarity.

There is some variation between the tensors, but most from the ceramic shards show oblateness, with applied fields in the orthogonal sample direction yielding smaller magnetizations than applied fields in the plane of the pot shard. This kind of "flattening" has been noticed previously in some studies of bricks and tiles[13,15]. The floors samples demonstrate little change in acquisition of TRM along the different axes and can arguably be considered isotropic.

AR2-MPB does not demonstrate the oblateness seen in the other samples. On re-inspection, it was found that this sample was not equidimensional and likely has a shape anisotropy (due to sample preparation of the limited material from this shard). The laboratory field during the Thellier-Coe experiment of the original sample was applied along the Z-axis of the sample; the Z-axis of the anisotropy test sample was ∼18% smaller than the largest axis (in this case, X). The application of this anisotropy tensor, therefore, cannot be considered appropriate.

A correction to the paleofield direction due to the TRM anisotropy is given by:

$$\hat{\mathbf{h}} = \frac{\boldsymbol{\kappa}^{-1}\hat{\mathbf{M}}}{|\boldsymbol{\kappa}^{-1}\hat{\mathbf{M}}|}. \tag{2}$$

Here, $\hat{\mathbf{M}}$ is a unit vector in the original NRM direction (which was found by applying principal component analysis to the stable final component of magnetization). Finally, $\boldsymbol{\kappa}$ and $\hat{\mathbf{h}}$ are used to calculate an intensity correction factor,

$$f_{An} = \frac{|\boldsymbol{\kappa}\hat{\mathbf{k}}|}{|\boldsymbol{\kappa}\hat{\mathbf{h}}|}, \tag{3}$$

where $\hat{\mathbf{k}}$ was the direction of the applied field during paleointensity experiments ($\hat{\mathbf{k}} = \{0, 0, 1\}$ for Thellier-Coe experiments on pot shards, and $\hat{\mathbf{k}} = \{1, 0, 0\}$ for Thellier-Coe experiments on floor samples). Values for f_{An} for floor samples would suggest a correction of less than 4%. For pot shards, corrections vary between $\sim$ 5-15% (ignoring the result from AR2-MPB).

Thellier-Coe results from ceramics meeting selection criteria are mainly from the Icon period (3 different pot shards). We examine the change in paleointensity variability given the anisotropy corrections. Three Thellier-Coe and 1 Shaw paleointensity estimate before TRM anisotropy correction yielded a mean paleointensity of 22.9 $\pm$ 2.00 μT. Correcting the Thellier-Coe results with the associated anisotropy correction factor and including the uncorrected Shaw result yields a new mean of 21.8 $\pm$ 1.80 μT.

Model Prediction Resolution. The age difference between the CALS3k.4 model[16] intensity dip (ca. 1500 AD) and the low intensity in the data is about 100 to 200 years. The ca. 1500 AD dip is seen in predictions from previous models incorporating sediment data (CALS3k.3[17]), and it deepens in the CALS3k.4 model (see Supplementary Figure 8). The datasets used for these models have no Southern Hemisphere archeomagnetic data within several thousand kilometers of our southern African sites (Supplementary Figure 8). We note that a model based on archeomagnetic data alone (ARCH3k.1[17]) predicts no anomalous low intensity at all. There are a few sediment sites that might contribute to the ca. 1500 intensity low predicted by the other models: 3 equatorial African sites, and a few lake sites in Argentina and Antarctica. It is well known that sediment ages can be too old due to the incorporation of ancient carbon. But in this case, the sediments appear to be predicting a low intensity at an age younger than that observed. Younger carbon can be introduced into a sediment, but this requires special, site specific conditions[19]. Moreover, we emphasize that the lake sediments yield only relative paleointensity information, and a calibration is needed for the incorporation of these data into models. Calibrated paleointensity values were apparently not used for the three equatorial African lake sites in the CALS3k.4 model (i.e. these are not listed in the relevant table source tables). There are a few more recent archeomagnetic results as old as 1550 AD from Brazil, but these are more than 7300 km from our sites.

In summary, the only Southern Hemisphere sites that could possibly contribute data to the 1500 AD predicted low intensity are vast distances from Africa. We conclude that the most up-to-date models (e.g. CALS3k.4) lack temporal resolution on time scales of 200 years for Southern Hemisphere African sites with ages older than the junction with models constrained by historical data (i.e. *gufm1*[20]). This resolution is insufficient to test the flux expulsion model we have proposed.

Supplementary References

1. Huffman, T., *Handbook to the Iron Age, The Archeology of Pre-Colonial Farming Societies in Southern Africa* (University of KwaZulu-Natel Press, Scottsville, South Africa), 504 pp., (2007).
2. Huffman, T.N., Intensive El Nino and the Iron Age of south-eastern Africa. *J. Archaeol. Sci.* **37**, 2572-2586 (2010).
3. Calabrese, J.A., *The Emergence of Social and Political Complexity in the Shashi-Limpopo Valley of Southern Africa, AD 900 to 1300, Ethnicity, Class and Polity.* (BAR International Series 1617, Archaeo Press, Oxford, 2007).
4. Hogg, A.G. et al., SHCal13 southern hemisphere calibration, 0-50,000 years cal BP. *Radiocarbon* **55**, 1889-1903 (2013).
5. Hanisch, E.O.M., Excavations at Icon, northern Transvaal. In Van der Merwe, N.J. & Huffman, T.N. (Eds.), *Iron Age Studies in Southern Africa.* (Goodwin Series 3, South African Archaeological Society, Cape Town, 1979).
6. Fouché, L., (Ed.), *Mapungubwe: Ancient Bantu Civilization on the Limpopo.* (Cambridge University Press, Cambridge, 1937).
7. Livingstone Smith, A., Bonfire II: The return of pottery firing temperatures, *J. Archeol. Sci.* **28**, 991-1003 (2001).
8. Winklhofer, M., Fabian, K., & Heider, F., Magnetic blocking temperatures of magnetite calculated with a three-dimensional micromagnetic model. *J. Geophys. Res.* **102**, 22695-22709 (1997).
9. Yu, Y., Importance of cooling rate dependence of thermoremanence in paleointensity determination. *J. Geophys. Res.* **116**, B09101 (2011).
10. Paterson, G. A., Tauxe, L., Biggin, A.J. Shaar, R. & Jonestrask, L.C., On improving the selection of Thellier-type paleointensity data, *Geochem. Geophys. Geosyst.* **15**, 1180-1192 (2014).
11. Coe, R.S., Grommé, C.G., & Mankinen, E.A., Geomagnetic paleointensities by the Thelliers' method from radiocarbon dated lava flows on Hawaii: The Pacific non-dipole low. *J. Geophys. Res.* **83**, 1740-1756 (1978).
12. Rogers, J., Fox, J.M.W. & Aitken, M.J., Magnetic anisotropy in ancient pottery. *Nature.* **277**, 644-646 (1979).
13. Aitken, M.J., Alcock, P.A., Bussel, G.D. & Shaw, C.J., Archaeomagnetic determination of the past geomagnetic intensity using ancient ceramics: allowance for anisotropy. *Archaeometry.* **23**, 53-64 (1981).
14. Veitch, R.J., Hedley, I.G. & Wagner, J.J., An investigation of the intensity of the geomagnetic field during Roman times using magnetically anisotropic bricks and tiles. *Arch. Sci. (Geneva).* **37**, 359-373 (1984).
15. Chauvin, A., Garcia, Y., Lanos, Ph. & Laubenheimer, F., Paleointensity of the geomagnetic field recovered on archaeomagnetic sites from France, *Phys. Earth. Planet. Int.* **120**, 111-136 (2000).

16. Korte, M. & Constable, C., Improving geomagnetic field reconstructions for 0-3 ka. *Phys. Earth Planet. Inter.* **188**, 247-259 (2011).

17. Donadini, F., Korte, M. & Constable, C. G., Geomagnetic field for 0-3ka: 1. New data sets for global modeling. *Geochem. Geophys. Geosyst.* **10**, Q06007 (2009).

18. Korte, M., Genevey, A., Constable, C.G., Frank, U., & Schnepp, E., Continuous geomagnetic field models for the past 7 millennia: 1. A new global data compilation. *Geochem. Geophys. Geosyst.* **6,** Q02H15 (2005).

19. Björck, S. & Wohlfarth, B., ^{14}C chronostratigraphic techniques in paleolimnology, In Last, W.M. & Smol, J.P., (Eds.), *Tracking Environmental Change Using Lake Sediments Volume 1: Basin Analysis, Coring, and Chronological Techniques.* (Kluwer, Academic Publishers, Dordrecht, The Netherlands. pp. 205-245, 2001).

20. Jackson, A., Jonkers, A.R.T., & Walker, M.R., Four centuries of geomagnetic secular variation from historical records. *Phil. Trans. Roy. Soc. London A.* **358**, 957-990 (2000).